Gas Breakdown and Discharge Formation in High-Power Impulse Magnetron Sputtering

Xiao Zuo, Rende Chen, Peiling Ke, and Aiying Wang

***Abstract*— Discharge behaviors of high-power impulse magnetron sputtering with different targets have been investigated. Distinct current–voltage curves and target current waveforms are observed. Breakdown voltage and the maximum target current show a periodic drop with the increase of atomic number in subgroups and periods. The target current density is found to be mainly affected by the secondary electron emission yield. Thus, its magnitude is unable to directly evaluate the ionization degree of sputtered atoms in high-power impulse magnetron sputtering (HiPIMS) process. In this paper, the interactive influence of secondary electron emission, sputter yield, and ionization energy on the ionization degree of sputtered atoms is discussed based on the analysis of the voltage and current characteristics. As a result, targets can be categorized into three sorts according to the ionization degree: 1) low ionization degree targets, such as Ag and C less than 10%; 2) intermediate ionization degree targets like Cr and Cu with 55% and 35%; 3) Ti, Zr, and Mo targets with the second ionization processes. These results provide institutive operation ranges for the state-of-the-art HiPIMS applications.**

***Index Terms*— Current waveform, gas breakdown, high-power impulse magnetron sputtering (HiPIMS), ionization degree, optical emission spectroscopy (OES).**

I. Introduction

BENIFITS from reduced electron energy loss and high instant discharge power, such as improved plasma density, ionization degree of sputtered atoms [1], and ion energy [2], make high-power impulse magnetron sputtering (HiPIMS) a hot topic in material engineering research studies and industrial applications. Many researchers consider it as a novel ionized physical vapor deposition technique [3] which takes advantages from dc magnetron sputtering (dcMS) and cathodic arc evaporation (CAE) in promoting substrate adhesion [4], film density [5], and surface smoothness [7], while avoiding the disadvantages from both of them like poor growth directionality, coarse columnar grain, and macroparticles. HiPIMS has already achieved great successes in microstructure modulation and property enhancement for thin films/coatings in laboratories [8]–[10]. However, its industrial application is still limited due to low deposition rate and discharge instability [11]–[13]. The loss of deposition rate attributes to the return of sputtered material ions back to target surface [14]. Meanwhile, discharge instability is also hard to avoid because HiPIMS works at abnormal glow region [16] which could easily transit into the arc region under high instant pulse voltage conditions [17]. Arcing on target surface will emit macrodroplets and degenerate thin films/coatings properties. These two features are the primary factors that need considering in HiPIMS applications.

According to specific applicable requirements, surface layers deposited by HiPIMS can be categorized into two main types: 1) surface protection coatings [18]–[20] and 2) functional thin films [7], [21], [22]. Surface protection coatings like transitional metal nitride/carbide are comprehensively deposited through dcMS or CAE methods. Their structures and properties are not quite sensitive to discharge instability unless pivotal mechanical damage caused by structural defects and property deterioration happens. Meanwhile, frequent arcing can be depressed by the advanced design of pulse unit [17]. However, the deposition rate of HiPIMS is much lower than dcMS, not even to mention CAE. Thus, although dense and refined grain nanocomposite coatings can be prepared by HiPIMS [8], [23], persuasion of coating customers turning into HiPIMS is not effective. However, low deposition rate does not matter so much to functional thin films, sometimes even becomes an advantage. Dutta *et al.* [25] reported that ultrathin Pt group metal films showed anomalous higher electric conductivity than Cu film. Film thickness can be controlled more precisely under low deposition rate conditions. Meanwhile, the high plasma density and ionization degree of sputtered atoms are beneficial to micronanoprocessing and the enhancement of film properties. For example, ions can be manipulated to fill or etch trenches and vias of semiconductor microprocessors [26], [27]. Ultrathin metal layers deposited by HiPIMS showed lower electrical resistivity than dcMS,

Manuscript received April 2, 2018; revised September 28, 2018; accepted December 20, 2018. This work was supported in part by the Project of the National Natural Science Foundation of China under Grant 11705258 and Grant 51522106, in part by the State Key Project of Fundamental Research of China under Grant 2017YFB0702303, in part by the Zhejiang Key Research and Development Program under Grant 2017C01001, in part by the Natural Science Foundation of Ningbo under Grant 2017A610012, and in part by the Cixi Municipal Key Technologies Research and Development Program under Grant 2015A07. The review of this paper was arranged by Senior Editor F. Taccogna. *(Corresponding authors: Peiling Ke; Aiying Wang.)*

X. Zuo, is with the Key Laboratory of Marine Materials and Related Technologies, Zhejiang Key Laboratory of Marine Materials and Protective Technologies, Ningbo Institute of Materials Technology and Engineering, Chinese Academy of Sciences, Ningbo 315201, China.

R. Chen is with the Key Laboratory of Marine Materials and Related Technologies, Zhejiang Key Laboratory of Marine Materials and Protective Technologies, Ningbo Institute of Materials Technology and Engineering, Chinese Academy of Sciences, Ningbo 315201, China, and also with the University of Chinese Academy of Sciences, Beijing 100049, China.

P. Ke and A. Wang are with the Key Laboratory of Marine Materials and Related Technologies, Zhejiang Key Laboratory of Marine Materials and Protective Technologies, Ningbo Institute of Materials Technology and Engineering, Chinese Academy of Sciences, Ningbo 315201, China, and also with the Center of Materials Science and Optoelectronics Engineering, University of Chinese Academy of Sciences, Beijing 100049, China (e-mail: kepl@nimte.ac.cn; aywang@nimte.ac.cn).

Color versions of one or more of the figures in this paper are available online at http://ieeexplore.ieee.org.

Digital Object Identifier 10.1109/TPS.2018.2889696

which has promising applications in microelectronics, space, and instrumentation technology [9], [28]. However, discharge instability like arcing would be vital for the properties of these kinds of thin films.

Therefore, considering the complex operation modes and particle transport processes [15], [29], [30], it is necessary to investigate the state-of-the-art operation ranges for various HiPIMS deposition applications. Helmersson and Samuelsson *et al.* [5] compared the deposition rate of eight different target materials (Al, Ti, Cr, Cu, Zr, Ag, Ta, and Pt) by HiPIMS with dcMS. Christie [14] analyzed the deposition rate for various sputtering targets by a pathway model. The ionization degree in the HiPIMS process with different targets under the same conditions differs. Moreover, Yushkov and Anders [6] found that gas breakdown in HiPIMS discharge was a function of the time to the previous discharge pulse. The discharge behaviors with various targets in HiPIMS need to be clarified. Herein, we will discuss the breakdown of Ar gas and discharge formation with Ag, Cu, Cr, Mo, Zr, Ti, and C targets. They are widely applied in the fabrication of diamond like carbon, carbon-based nanocomposites, and transitional metal nitride coatings. The sputter yield and ionization energy of these targets vary in large ranges. The voltage and current characteristics are analyzed to find the contribution of four processes on HiPIMS discharge, such as secondary electron emission, gas sputter, self-sputter, and ionization of sputtered materials. Especially the interactive influence of secondary electron emission yield, sputter yield and ionization energy on the ionization degree of sputtered materials are clarified. Optical emission spectroscopy (OES) further conforms the results of the analysis. Finally, a probable application scope of HiPIMS deposition concerning ionization degree of sputtered materials and deposition rate is suggested.

II. Experimental Setup and Target Current

A. Experimental Setup

Details about the HiPIMS equipment and target current measurement arrangements have been described in [16]. The dimensions of the cylindrical chamber are 60 cm in diameter and 60 cm in height. Background pressure for all experiments is pumped to 1.5×10^{-2} mTorr to avoid the influence from residual oxygen and water molecule to the utmost. Working pressure is set at 3.8 mTorr by 50-sccm research grade (99.999%) Ar gas. A pulse unit (HPPMS-20k, PTL) is used to power the magnetron. Pulsewidth and pulse frequency are 200 μs and 50 Hz, respectively. The targets (99.9% purity with the size of 40 cm × 10 cm × 0.7 cm) with various sputter yields are used to investigate target current behaviors with the variation of the pulse voltage. Gas sputter yield (Y_{Ar^+}) and self-sputter yield (Y_{self}) under different incident energy (E_i) ion bombardments are calculated by SRIM [31], which are plotted in Fig. 1. OES (Acton SpectraPro SP-2500, Princeton Instruments) is applied to characterize particle species and emission intensities, which scans from 200 to 900 nm with wavelength resolution of 1 nm. Although it is the plasma region near the substrate holder measured by OES, its results still could provide reliable references for discussion.

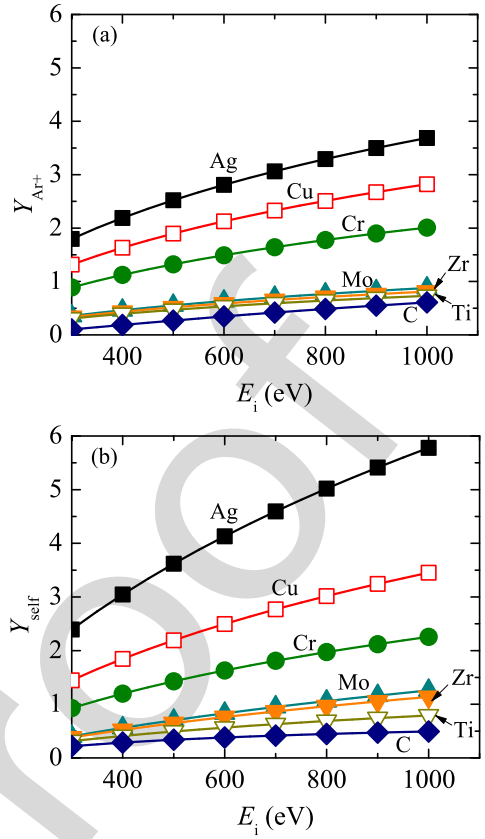

Fig. 1. (a) Sputter yield (Y_{Ar^+}) and (b) self-sputter yield (Y_{self}) of the targets under different incident ion energies (E_i). (Obtained by SRIM software.)

Meanwhile, it should be noted that the OES data just give qualitative information on HiPIMS discharge.

B. About Target Current

Average target currents (I_{ave}) during each pulse were calculated by the following formula:

$$I_{ave} = \frac{1}{T}\int_0^T I_t(t)dt \tag{1}$$

where T = 20 ms is the pulse period.

The target current generated from Ar^+ incidence (I_{Ar^+}), including ion current and secondary electron current, can be written in the following equation:

$$I_{Ar^+} = 0.5eSn_{Ar^+}(1+\gamma_{Ar^+})\sqrt{\frac{k_B T_e}{m_{Ar^+}}} \tag{2}$$

where e is the elementary charge, S is the area of racetrack, n_{Ar^+} is the density of Ar^+ ions, γ_{Ar^+} is the secondary electron emission yield under the bombardment of Ar^+, k_B is Boltzmann's constant, T_e is the electron temperature, and m_{Ar^+} is the mass of Ar^+. Current generated from sputtered material ions ($I_{M^{z+}}$) can also be written in similar equations as follows:

$$I_{M^{z+}} = \sum_{z=1,2} zeS\Gamma_{M^{z+}}(1+\gamma_{M^{z+}}) \tag{3}$$

$$\Gamma_{M^+} = 0.5\alpha(Y_{Ar^+}n_{Ar^+} + Y_{self}n_{M^+} + Y_{self}{}'n_{M^{2+}})\sqrt{\frac{k_B T_e}{m_{M^+}}} \quad (4)$$

$$\Gamma_{M^{2+}} = 0.5\beta(Y_{Ar^+}n_{Ar^+} + Y_{self}n_{M^+} + Y_{self}{}'n_{M^{2+}})\sqrt{\frac{k_B T_e}{m_{M^{2+}}}} \quad (5)$$

where $\Gamma_{M^{z+}}$ is the metal ion flux to the target, α ($0 < \alpha < 1$) is the first ionization degree of the target material, β is the second ionization degree, $Y_{self}{}'$ is self-sputter yield under M^{2+} ions, n_{M^+} and $n_{M^{2+}}$ are M^+ and M^{2+} density, respectively, and $m_{M^+} = m_{M^{2+}}$ is the target material ion mass. Therefore, the target current (I_t) can be obtained: $I_t = I_{Ar^+} + I_{M^{z+}}$. For simplicity, first, without considering the second ionization of sputtered material atoms, I_t can be written as the following form:

$$I_t = eS\Gamma_{Ar^+}\left(1 + \gamma_{Ar^+} + \frac{\alpha Y_{Ar^+}}{2 - \alpha Y_{self}}\sqrt{\frac{m_{Ar^+}}{m_{M^+}}}\right) \quad (6)$$

where Γ_{Ar^+} is the Ar^+ ion flux to target, which is expressed as follows:

$$\Gamma_{Ar^+} = 0.5 n_{Ar^+}\sqrt{\frac{k_B T_e}{m_{M^+}}}. \quad (7)$$

III. Results and Discussion

A. Breakdown Voltage and Pulse Voltage Range of Different Targets in Ar HiPIMS

The current–voltage (*IV*) curves of HiPIMS with various targets are shown in Fig. 2. Pulse voltage is the set output voltage of the power supply, while voltage measured on the target by the oscilloscope is labeled as the target voltage. When the target voltage is high enough to ionize the Ar gas, gas breakdown and discharge occur. The breakdown voltages (U_b) of Ar gas in HiPIMS with different targets are distinct, which are plotted in Fig. 3. Breakdown voltage for graphite (C) target is the highest (721 V), while for Zr target is the lowest (356 V). The averaged target current increases with the improvement of the pulse voltage. However, too much high pulse voltage results in arc. The arcing voltages (U_{arc}) for each kind of targets are presented in Fig. 3. When the pulse voltage is higher than those values for a specific target, arcs generate. Thus, the stable work ranges of pulse voltage are obtained. Zr and Mo targets are sputtered in wider voltage ranges than others. Zr target can work in the largest voltage range, but the highest pulse voltage is achieved on the Mo target. In addition, Ti, Cu, and W targets can also work stably in large voltage ranges. However, Ag HiPIMS discharges easily transform from glow into arc.

As it is known, breakdown voltage is defined as the lowest voltage at which electric discharge occurs. It is determined by the work function (F) of the targets, which is the minimum energy needed to remove an electron from the target into the vacuum. Thus, it is expected that the variation of breakdown voltage with atomic number (Z) has a similar trend like work function. However, although the work function determines the breakdown voltage of various targets, it does not show a direct relationship with arcing voltage. In the process of glow discharge formation, energetic electrons emitted from target surface ionize Ar atoms in avalanche forms. In this stage, sputtering has not happened yet. When the generated ions are attracted back to bombard target surface energetically, sputtering happens. In HiPIMS discharge, the atoms emitted from the target surface are thought to be ionized overwhelmingly as compared to dcMS [1]. This process even can dominate in HiPIMS, which is able to cause severe self-sputter [30]. Discharge state in this stage is affected by target materials greatly. Therefore, arcing voltage would be influenced by the ionization of sputtered materials.

Meanwhile, no direct relationship between target current and sputter yield is observed as shown in Fig. 2. The averaged current is the lowest on Ag target that has the highest sputter yield. When the pulse voltage is 700 V, the average current of different targets is in the order from high to low as follows: Ti, Zr, Mo, Cu, Ag, and C. In addition, with the increase in pulse voltage, *IV* curves present different slopes which can be classified into two groups. For example, the Cu target current increases slowly after breakdown, and then, with the increase in pulse voltage, it becomes more and more fast until arc happens. However, the increase tendency of target current with pulse voltage for Ti is on the contrary. These differences from *IV* curves indicate that the secondary electron emission yield, gas sputter yield, self-sputter yield, and ionization energy will affect the discharge in HiPIMS interactively.

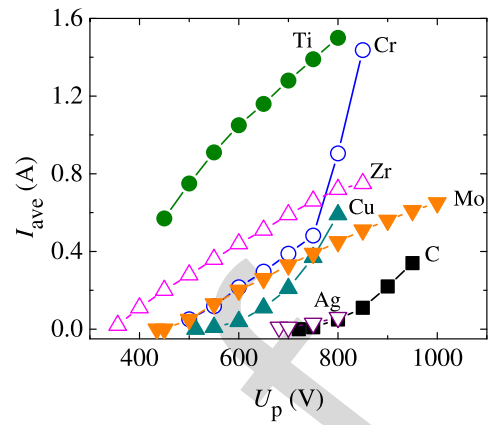

Fig. 2. Variations of averaged target current (I_{ave}) with pulse voltage (U_p) in HiPIMS discharges with different targets (measured).

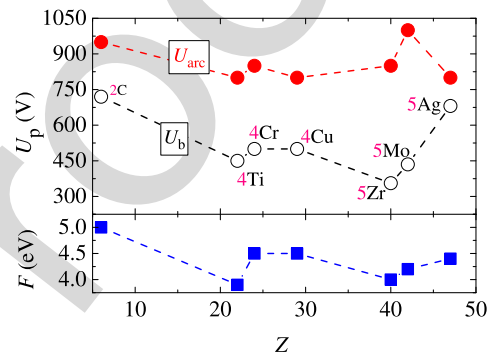

Fig. 3. Variation of breakdown voltage (U_b), arcing voltage (U_{arc}), and work function (F) with atomic number (Z).

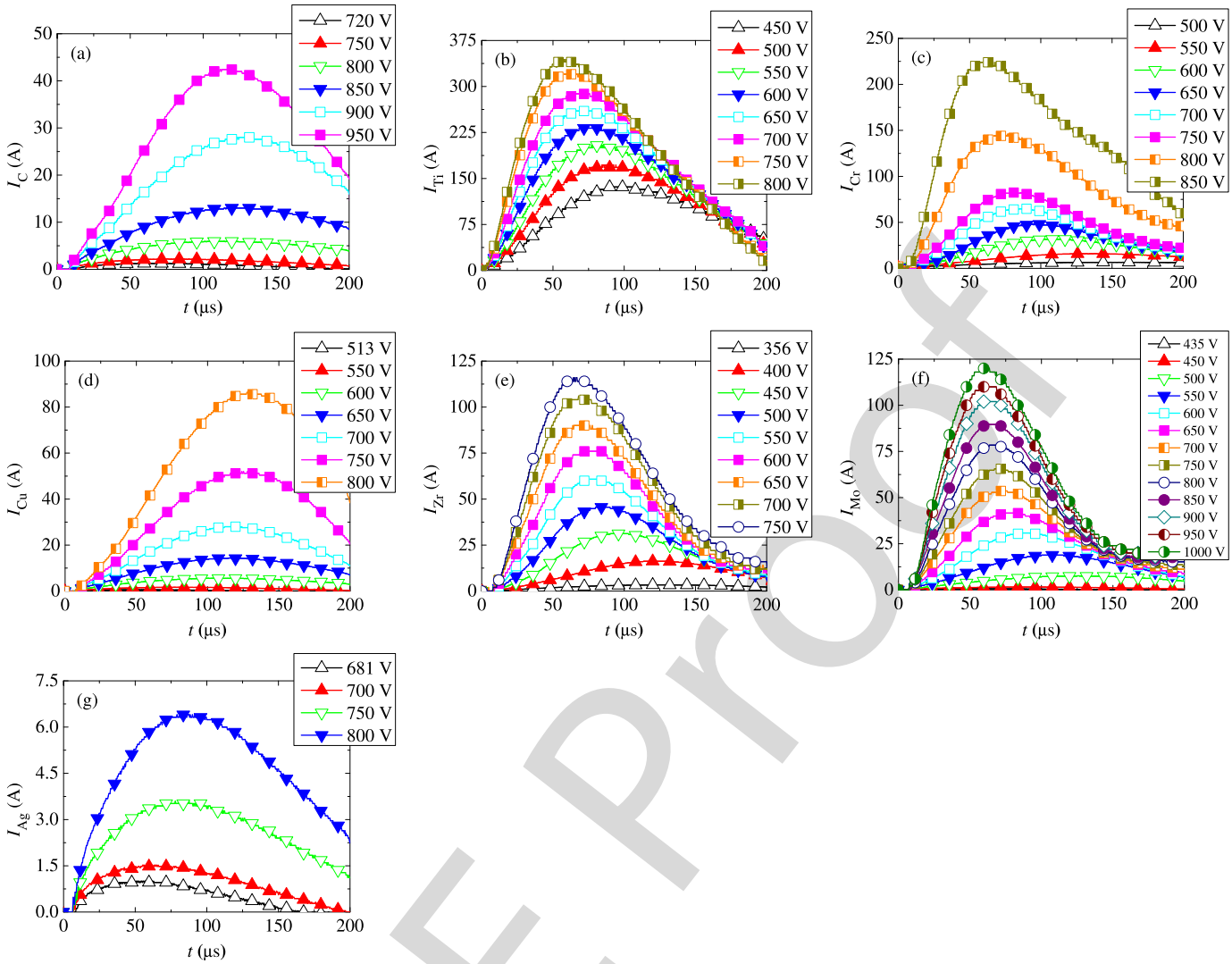

Fig. 4. Different target current waveforms in the pulse voltage ranges of stable HiPIMS discharges. Current measured on the C, Ti, Cr, Cu, Zr, Mo, and Ag targets is labeled as I_C, I_{Ti}, I_{Cr}, I_{Cu}, I_{Zr}, I_{Mo}, and I_{Ag}, respectively.

B. Variation of Current Waveform on Different Targets

The current waveforms on different targets during the 200-μs pulse-on time are demonstrated in Fig. 4. Apparently, all the target currents are transient. No stable current stage is observed. Although all the current waveforms present humplike shape, some details in current behaviors are distinct for different targets. First, I_{Zr} and I_{Mo} can nearly reach a stable low current stage at the end of relatively high-voltage pulse conditions ($\geq$500 and 600 V, respectively). Second, the time (Δt_{max}) of target current maximum (I_p) changes with pulse voltage and differs in target elements. Δt_{max} increases with the rise of pulse voltage on Cu and Ag targets but decreases on other targets in our experiments. Third, the target current at the same pulse voltage is also different. The current waveform is interactive resultant of ionization, gas sputter, self-sputter, and gas rarefaction processes. Its evolution under various conditions has been discussed in detail by many researchers [32]–[34]. Here, we focus on the target current maximum as it is a key parameter affecting the sputtering rate. Usually, high target current is preferred in HiPIMS unless arc generates. The highest current is obtained on Ti target in our experiments when the same pulse voltage (700 V) is applied. Details of target current waveform, including current maximum, Δt_{max}, increment rate (k_u), and decreasing rate (k_d) at 700 V for different targets, are presented in Fig. 5. The pulse voltage applied on the graphite target is selected as 720 V, because 700 V is insufficient for discharge formation. For targets with transitional metal in a subgroup (III or IV) or period (third or fourth), target current maximum decreases with the increase in atomic number. Fig. 5(b) shows the change of Δt_{max} with different atomic numbers. However, Fig. 5(b) does not show a similar trend like current maximum in Fig. 5(a). This could attribute to the ionization of sputtered materials. k_u and k_d are defined in the following equations:

$$k_u = \frac{I_p - 0}{\Delta t_{max}} \tag{8}$$

$$k_d = \frac{I_{end} - I_p}{200 - \Delta t_{max}} \tag{9}$$

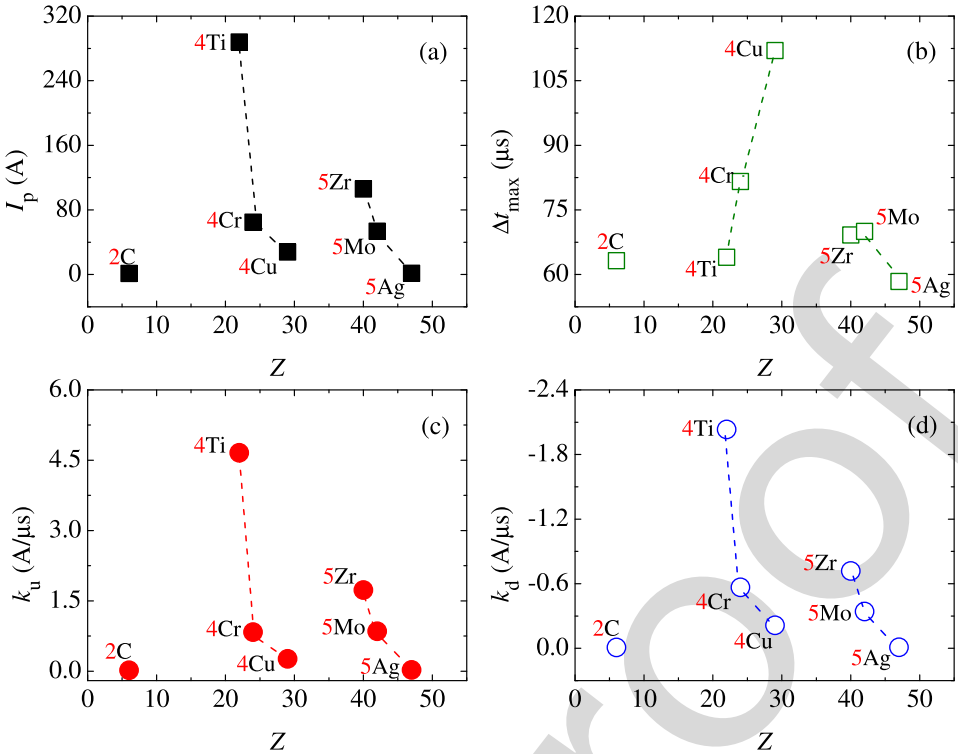

Fig. 5. Details on the current waveforms on different targets measured at with pulse voltage at 700 V, such as (a) current maximum (I_p), (b) corresponding time (Δt_{max}), (c) increase rate (k_u), and (d) decrease rate (k_d).

where I_{end} is the target current at the end of voltage pulse. As shown in (6), the rate of change in target current generally presents the ionization rate in HiPIMS discharge. It is found that for HiPIMS discharge with higher current maximum, the target current reaches maximum faster, but also decreases earlier. k_u and k_d also obey periodic feature like I_p. Generally, k_d is smaller than k_u. The change trend of them with atomic number is similar with the secondary electron emission yield except Ti.

When working pressure and pulse voltage are the same, secondary electron emission yield on different targets will lead to significant distinct in plasma density in HiPIMS. Thus, the dose of incident Ar^+ on the targets changes with different target elements. The incident Ar^+ generates new electrons and sputters target atoms out. The sputtered atoms will also be ionized in HiPIMS plasma. The target current is a sum of conductive electron current and ion current. Ion current composes of Ar^+ current and target material ions current. There would be monovalent and bivalent ions of target material according to first ionization energy ($E_{0\to1}$) and second ionization energy ($E_{1\to2}$). The electron current on the target surface is generated from Ar^+ and target material ions. The density of target material ions is influenced by Y_{Ar^+}, Y_{self}, $E_{0\to1}$, and $E_{1\to2}$. When we analyze the target current, the difference in secondary electron emission yield is considered first. Fig. 6 figures out the change of secondary electron emission yield (γ_{SEEY}) with atomic number corresponding to different target materials. The incident ion energy is assumed to be 700 eV when the pulse voltage is 700 V. As the energy per atomic mass number is less than 300 eV, secondary electron emission is determined by the potential energy (E_p) of incident ions [30]. Therefore, the secondary electron yield from ion bombardment can be calculated by the following equation:

$$\gamma_{SEEY} = 0.032 * (0.78E_p - 2F). \tag{10}$$

The values of work function (F) and potential energy (E_p) for different materials are listed in Table I. As shown in Fig. 6(a), with the increase in atomic number in a subgroup or period, γ_{Ar^+} has a similar trend like the target current maximum in Fig. 5(a). It means that the electron current generated by Ar^+ incidence is dominant. However, when carefully comparing γ_{Ar^+} of the elements from the fourth period with that of the fifth period, Zr HiPIMS should have the highest target current at the same pulse voltage. However, current on Ti target is the highest; meanwhile, Cr and Cu

TABLE I

F, FIRST, AND SECOND IONIZATION ENERGIES FOR VARIOUS MATERIALS

Element	F (eV)	$E_{0\to1}$ (eV)	$E_{1\to2}$ (eV)
Ar	N/A	15.76	27.63
C	4.5	11.26	24.38
Ti	3.9	6.83	13.58
Cr	4.5	6.77	16.5
Cu	4.9	7.73	20.29
Zr	4.0	6.63	13.16
Mo	4.2	7.09	16.17
Ag	4.4	7.58	21.45

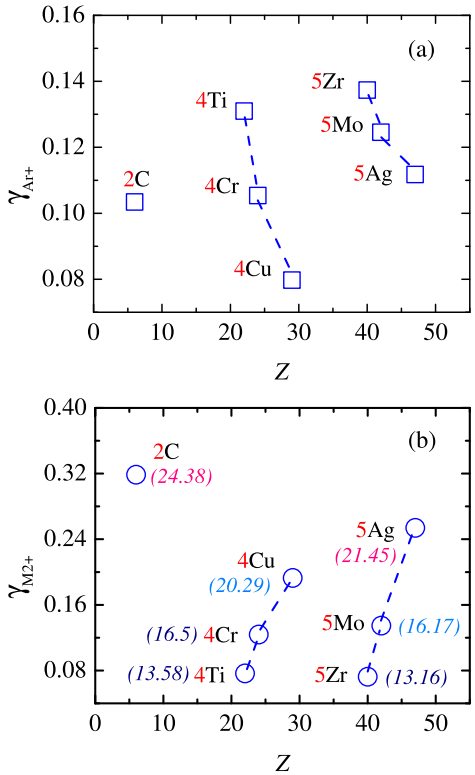

Fig. 6. Secondary electron emission yield (γ_{SEEY}) of various targets under the bombardment of (a) Ar^+ ions and (b) bivalent target material ions (M^{2+}).

HiPIMS also have higher target current than Mo and Ag HiPIMS, respectively. Since the monovalent ions are unable to cause secondary electron emission, the existence of bivalent target material ions is further considered. The first ionization energy of Ar is 15.76 eV, and target material atoms with the second ionization energy lower than 15.76 eV, like Ti and Zr, can be ionized into bivalent ions with high probability. In addition, there are Cr and Mo that have the second ionization energies near around 15.76 eV. These sputtered materials participated in discharge processes and are partially ionized. Therefore, different sputter yield and ionization degrees would also contribute to the variation deviation of target current maximum from γ_{Ar^+}.

C. Relationship Between Ionization Degree and Peak Target Current

As the working pressure is set at 3.8 mTorr, the mean free path is larger than cathode sheath thickness. Therefore, when the pulse voltage is 700 V, it is reasonable to assume that the energy of incident ions is 700 eV as the second ionization process is neglected. Gas sputter yield and self-sputter yield of various targets with incident energy at 700 eV can be found in Fig. 1. Self-sputter yield is higher than the gas sputter yield. The difference between them is distinct according to the kind of target material. For Ag and Cu targets, the self-sputter yield is much higher than gas sputter yield when compared with others. It could be speculated that the target material with high ionization degree, self-sputter yield, and low ionization energy

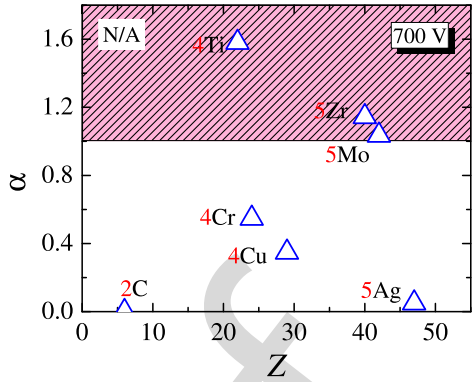

Fig. 7. Calculated ionization degree (α) of various target materials. The second ionization process exists when α is larger than 1.

prefers the state-of-the-art HiPIMS with high deposition rate and stability.

As the target current is transit, the ionization degree of sputtered materials is also expected to vary with time. The ionization degree can be calculated through the ionization region model [33]. The cross section data of excitation, ionization, deexcitation, and combination processes for different species can be found in reaction databases, such as from the OpenADAS database [35]. When the pulse voltage and working pressure are 700 V and 3.8 mTorr, the maximums of ionization degree (α) calculated from different target currents are presented in Fig. 7. According to these maximums of ionization degree, target materials can be categorized into three kinds: 1) Ag and C targets, the maximum ionization degree is less than 10%; 2) 55% and 35% for Cr and Cu; and 3) higher than 100% for Ti, Zr, and Mo. The ionization energy of C atom is the highest, thus its ionization degree is the lowest. However, the ionization energy of Ag atom is lower than that of Cu atoms, but its ionization degree is also very low. This phenomenon can be attributed to its high sputter yield, a large amount of Ag atoms participate in discharge which would reduce the electron temperature. Therefore, the target with high sputter yield will have a reduced ionization degree. Ionization degree higher than 100% is impossible, and these results are attributed to that only the first ionization processes are considered and bivalent ions are neglected. It is easy to deduce that the second ionization process exists in Ti, Zr, and Mo HiPIMS. Therefore, it is expectable to control the incident particles' energy to design dense, fine grain, and nanocomposite films for Cr, Ti, Zr, and Mo targets but obtain relatively high deposition rate for Ag and Cu targets in HiPIMS deposition process. For the high ionization energy and low sputter yield target C, other methods should be introduced to improve ionization degree [36] or deposition rate [37]. These results can also be explored to other targets according to their secondary electron emission yield, sputter yield, and ionization degree with the exception of ferromagnetic materials such as Fe, Co, and Ni.

D. Optical Emission Spectra of C, Cr, and Ti HiPIMS Plasma

According to the first and second ionization of sputtered atoms, OES spectra for HiPIMS with three different targets

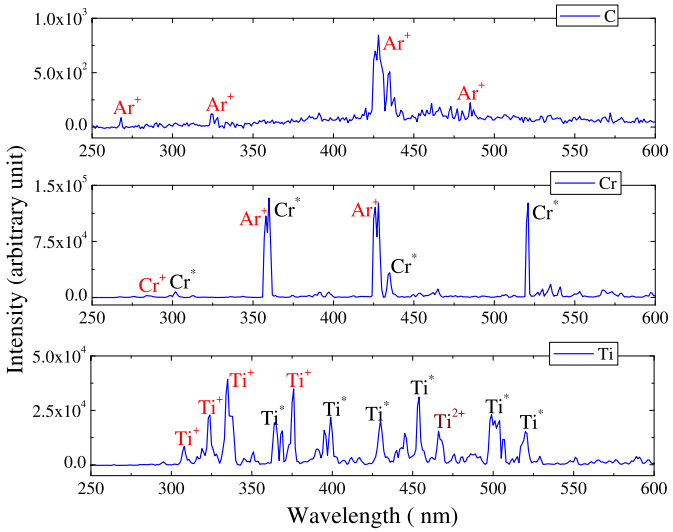

Fig. 8. OES spectra of C, Cr, and Ti HiPIMS discharge.

are detected, such as high first ionization energy element C, low second ionization energy element Ti, and high sputter yield element Cr. Correspondingly, the pulse voltage and pressure for OES measurements are 700 V and 3.8 mTorr, respectively. All the parameters of the spectroscope are set the same so that the measured OES spectra can be comparable with each other. The results are plotted in Fig. 8. C atom spectrum cannot be found. A weak spectrum peak of CrII 284 nm appears in the OES spectra of Cr HiPIMS discharge. As predicted from the ionization degree analysis, TiIII 466 nm of bivalent Ti^{2+} ions were observed in Ti HiPIMS.

IV. Conclusion

The discharge behaviors of HiPIMS have been investigated on Ag, Cu, Cr, Mo, Zr, Ti, and C targets. The breakdown voltage is determined by the work function of the target element, but the arcing voltage is also affected by the ionization of sputtered atoms. Stable discharge ranges of these targets are found. High Γ_{SEEY} results in low breakdown voltage and high discharge current, and vice versa. HiPIMS discharge with Ti, Mo, and Zr targets is not easy to arc at high voltage. An analytical current model was used to analyze the interactive influence of the secondary electron emission yield, sputter yield, and ionization energy on the ionization degree of sputtered atoms. The results show that the target materials with relatively low ionization energy and sputter yield, such as Cr, Ti, Zr, and Mo, tend to have higher ionization degree. Targets with high sputter yield like Ag and Cu have low ionization degree. The second ionization of sputtered atoms happens in Ti, Zr, and Mo HiPIMS. However, high sputter yield elements like Ag and Cu have relatively low ionization degree.

References

[1] D. Lundin, M. Čada, and Z. Hubička, "Ionization of sputtered Ti, Al, and C coupled with plasma characterization in HiPIMS," *Plasma Sources Sci. Technol.*, vol. 24, p. 035018, Jun. 2015.

[2] A. Hecimovic and A. P. Ehiasarian, "Time evolution of ion energies in HIPIMS of chromium plasma discharge," *J. Phys. D: Appl. Phys.*, vol. 42, no. 13, p. 135209, 2009.

[3] U. Helmersson, M. Lattemann, J. Bohlmark, A. P. Ehiasarian, and J. T. Gudmundsson, "Ionized physical vapor deposition (IPVD): A review of technology and applications," *Thin Solid Films*, vol. 513, pp. 1–24, Aug. 2006.

[4] Z. Wang, D. Zhang, P. Ke, X. Liu, and A. Wang, "Influence of substrate negative bias on structure and properties of TiN coatings prepared by hybrid HIPIMS method," *J. Mater. Sci. Technol.*, vol. 31, no. 1, pp. 37–42, 2015.

[5] M. Samuelsson, D. Lundin, J. Jensen, M. A. Raadu, J. T. Gudmundsson, and U. Helmersson, "On the film density using high power impulse magnetron sputtering," *Surf. Coat. Technol.*, vol. 205, no. 2, pp. 591–596, 2010.

[6] G. Y. Yushkov and A. Anders, "Origin of the delayed current onset in high-power impulse magnetron sputtering," *IEEE Trans. Plasma Sci.*, vol. 38, no. 11, pp. 3028–3034, Nov. 2010.

[7] F. Cemin *et al.*, "Epitaxial growth of Cu(001) thin films onto Si(001) using a single-step HiPIMS process," *Sci. Rep.*, vol. 7, May 2017, Art. no. 1655.

[8] P. Souček *et al.*, "Superhard nanocomposite nc-TiC/aC:H coatings: The effect of HiPIMS on coating microstructure and mechanical properties," *Surf. Coat. Technol.*, vol. 311, pp. 257–267, Feb. 2017.

[9] F. Cemin, D. Lundin, D. Cammilleri, T. Maroutian, P. Lecoeur, and T. Minea, "Low electrical resistivity in thin and ultrathin copper layers grown by high power impulse magnetron sputtering," *J. Vac. Sci. Technol. A, Vac., Surf., Films*, vol. 34, no. 5, p. 051506, 2016.

[10] X. Qin, P. Ke, A. Wang, and K. H. Kim, "Microstructure, mechanical and tribological behaviors of MoS_2-Ti composite coatings deposited by a hybrid HIPIMS method," *Surf. Coat. Technol.*, vol. 228, pp. 275–281, Aug. 2013.

[11] P. Raman, J. Weberski, M. Cheng, I. Shchelkanov, and D. N. Ruzic, "A high power impulse magnetron sputtering model to explain high deposition rate magnetic field configurations," *J. Appl. Phys.*, vol. 120, no. 16, p. 163301, 2016.

[12] N. Brenning *et al.*, "Understanding deposition rate loss in high power impulse magnetron sputtering: I. Ionization-driven electric fields," *Plasma Sources Sci. Technol.*, vol. 21, no. 2, p. 025005, 2012.

[13] K. Yukimura, R. Mieda, H. Tamagaki, and T. Okimoto, "Electrical characteristics of arc-free high-power pulsed sputtering glow plasma," *Surf. Coat. Technol.*, vol. 202, pp. 5246–5250, Aug. 2008.

[14] D. J. Christie, "Target material pathways model for high power pulsed magnetron sputtering," *J. Vac. Sci. Technol. A, Vac., Surf., Flims*, vol. 23, no. 2, pp. 330–335, 2005.

[15] N. Brenning, J. T. Gudmundsson, M. A. Raadu, T. J. Petty, T. Minea, and D. Lundin, "A unified treatment of self-sputtering, process gas recycling, and runaway for high power impulse sputtering magnetrons," *Plasma Sources Sci. Technol.*, vol. 26, no. 12, p. 125003, 2017.

[16] X. Zuo, P. Ke, R. Chen, X. Li, M. Odén, and A. Wang, "Discharge state transition and cathode fall thickness evolution during chromium HiPIMS discharge," *Phys. Plasmas*, vol. 24, p. 083507, Jul. 2017.

[17] D. J. Christie, F. Tomasel, W. D. Sproul, and D. C. Carter, "Power supply with arc handling for high peak power magnetron sputtering," *J. Vac. Sci. Technol. A, Vac., Surf., Films*, vol. 22, no. 4, pp. 1415–1419, 2004.

[18] X. Tian, Y. Ma, J. Hu, M. Bi, C. Gong, and P. K. Chu, "Microstructure and mechanical properties of $(AlTi)_xN_{1-x}$ films by magnetic-field-enhanced high power impulse magnetron sputtering," *J. Vac. Sci. Technol. A, Vac., Surf., Films*, vol. 35, p. 021402, Mar. 2017.

[19] S. Danaher, T. Dudziak, P. K. Datta, R. Hasan, and P. S. Leung, "Long-term oxidation of newly developed HIPIMS and PVD coatings with neural network prediction modelling," *Corrosion Sci.*, vol. 69, pp. 322–337, Apr. 2013.

[20] K. D. Bakoglidis *et al.*, "Comparative study of macro- and microtribological properties of carbon nitride thin films deposited by HiPIMS," *Wear*, vols. 370–371, pp. 1–8, Jan. 2017.

[21] A. Aijaz, Y.-X. Ji, J. Montero, G. A. Niklasson, C. G. Granqvist, and T. Kubart, "Low-temperature synthesis of thermochromic vanadium dioxide thin films by reactive high power impulse magnetron sputtering," *Sol. Energy Mater. Sol. Cells*, vol. 149, pp. 137–144, May 2016.

[22] M. Mickan, U. Helmersson, H. Rinnert, J. Ghanbaja, D. Müller, and D. Horwat, "Room temperature deposition of homogeneous, highly transparent and conductive Al-doped ZnO films by reactive high power impulse magnetron sputtering," *Sol. Energy Mater. Sol. Cells*, vol. 157, pp. 742–749, Dec. 2016.

[23] Q. Ma, L. Li, Y. Xu, J. Gu, L. Wang, and Y. Xu, "Effect of bias voltage on TiAlSiN nanocomposite coatings deposited by HiPIMS," *Appl. Surf. Sci.*, vol. 392, pp. 826–833, Jan. 2017.

[24] D. Lundin, J. Jensen, and H. Pedersen, "Influence of pulse power amplitude on plasma properties and film deposition in high power pulsed plasma enhanced chemical vapor deposition," *J. Vac. Sci. Technol. A, Vac., Surf., Films*, vol. 32, p. 030602, Mar. 2014.

[25] S. Dutta *et al.*, "Thickness dependence of the resistivity of platinum-group metal thin films," *J. Appl. Phys.*, vol. 122, p. 025107, Jul. 2017.

[26] A. Anders, "Metal plasmas for the fabrication of nanostructures," *J. Phys. D: Appl. Phys.*, vol. 40, no. 8, p. 2272, 2007.

[27] H. L. Brown, S. A. Thornley, S. J. Wakeham, M. J. Thwaites, R. J. Curry, and M. A. Baker, "The impact of substrate bias on a remote plasma sputter coating process for conformal coverage of trenches and 3D structures," *J. Phys. D: Appl. Phys.*, vol. 48, no. 33, p. 335303, 2015.

[28] A. A. Solovyev, V. A. Semenov, V. O. Oskirko, K. V. Oskomov, A. N. Zakharov, and S. V. Rabotkin, "Properties of ultra-thin Cu films grown by high power pulsed magnetron sputtering," *Thin Solid Films*, vol. 631, pp. 72–79, Jun. 2017.

[29] K. Sarakinos, J. Alami, and S. Konstantinidis, "High power pulsed magnetron sputtering: A review on scientific and engineering state of the art," *Surf. Coat. Technol.*, vol. 204, no. 11, pp. 1661–1684, 2010.

[30] A. Anders, J. Andersson, and A. Ehiasarian, "High power impulse magnetron sputtering: Current-voltage-time characteristics indicate the onset of sustained self-sputtering," *J. Appl. Phys.*, vol. 102, no. 11, p. 113303, 2007.

[31] J. F. Ziegler, M. D. Ziegler, and J. P. Biersack, "SRIM—The stopping and range of ions in matter (2010)," *Nucl. Instrum. Methods Phys. Res. B, Beam Interact. Mater. At.*, vol. 268, pp. 1818–1823, Jun. 2010.

[32] Z. Wu *et al.*, "Discharge current modes of high power impulse magnetron sputtering," *AIP Adv.*, vol. 5, no. 9, p. 097178, 2015.

[33] M. Raadu, I. Axnäs, J. T. Gudmundsson, C. Huo, and N. Brenning, "An ionization region model for high-power impulse magnetron sputtering discharges," *Plasma Sources Sci. Technol.*, vol. 20, no. 6, p. 065007, 2011.

[34] B. C. Zheng, Z. L. Wu, B. Wu, Y. G. Li, and M. K. Lei, "A global plasma model for reactive deposition of compound films by modulated pulsed power magnetron sputtering discharges," *J. Appl. Phys.*, vol. 121, no. 17, p. 171901, 2017.

[35] H. P. Summers and M. G. O'Mullane, "Atomic data and modelling for fusion: The ADAS project," in *Proc. AIP Conf.*, vol. 1, 2011, pp. 179–187.

[36] A. Aijaz *et al.*, "Synthesis of hydrogenated diamondlike carbon thin films using neon–acetylene based high power impulse magnetron sputtering discharges," *J. Vac. Sci. Technol. A, Vac., Surf., Films*, vol. 34, no. 6, p. 061504, 2016.

[37] M. Hiratsuka, A. Azuma, H. Nakamori, Y. Kogo, and K. Yukimura, "Extraordinary deposition rate of diamond-like carbon film using HIPIMS technology," *Surf. Coat. Technol.*, vol. 229, pp. 46–49, Aug. 2013.

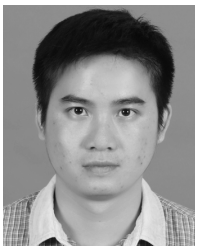

Xiao Zuo received the B.S. degree in physics from Hunan Normal University, Changsha, China, in 2009, and the Ph.D. degree in plasma physics from the Institute of Plasma Physics, Chinese Academy of Sciences, Hefei, China, in 2014.

His current research interests include high-power impulse magnetron sputtering discharge, plasma diagnosis, and simulation.

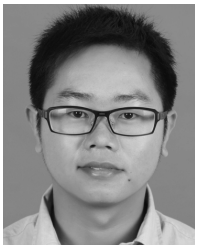

Rende Chen received the B.S. degree in communication engineering from the Beijing Institute of Petrochemical Technology, Beijing, China, in 2010, and the M.S. degree in material science and engineering from the University of Chinese Academy of Sciences, Beijing, China.

He is currently with the Ningbo Institute of Material Technology and Engineering, Chinese Academy of Sciences, Ningbo, China, where he is involved in the research work. His current research interests include vacuum technologies and plasma diagnosis.

Peiling Ke received the Ph.D. degree from the Institute of Metal Research, Chinese Academy of Sciences, Shenyang, China, in 2006.

Her current research interests include novel solid lubricant materials, MAX phase coatings, high-power impulse magnetron sputtering coating processes, and so on.

Aiying Wang received the B.S. degree in material science and engineering from Northwestern Polytechnical University, Xi'an, China, in 1998, and the Ph.D. degree from the Institute of Metal Research, Chinese Academy of Sciences, Shenyang, China, in 2003.

Her current research interests include advanced carbon-based materials, materials simulation, plasma surface engineering, and so on.

Gas Breakdown and Discharge Formation in High-Power Impulse Magnetron Sputtering

Xiao Zuo, Rende Chen, Peiling Ke, and Aiying Wang

***Abstract*— Discharge behaviors of high-power impulse magnetron sputtering with different targets have been investigated. Distinct current–voltage curves and target current waveforms are observed. Breakdown voltage and the maximum target current show a periodic drop with the increase of atomic number in subgroups and periods. The target current density is found to be mainly affected by the secondary electron emission yield. Thus, its magnitude is unable to directly evaluate the ionization degree of sputtered atoms in high-power impulse magnetron sputtering (HiPIMS) process. In this paper, the interactive influence of secondary electron emission, sputter yield, and ionization energy on the ionization degree of sputtered atoms is discussed based on the analysis of the voltage and current characteristics. As a result, targets can be categorized into three sorts according to the ionization degree: 1) low ionization degree targets, such as Ag and C less than 10%; 2) intermediate ionization degree targets like Cr and Cu with 55% and 35%; 3) Ti, Zr, and Mo targets with the second ionization processes. These results provide institutive operation ranges for the state-of-the-art HiPIMS applications.**

***Index Terms*— Current waveform, gas breakdown, high-power impulse magnetron sputtering (HiPIMS), ionization degree, optical emission spectroscopy (OES).**

I. Introduction

BENIFITS from reduced electron energy loss and high instant discharge power, such as improved plasma density, ionization degree of sputtered atoms [1], and ion energy [2], make high-power impulse magnetron sputtering (HiPIMS) a hot topic in material engineering research studies and industrial applications. Many researchers consider it as a novel ionized physical vapor deposition technique [3] which takes advantages from dc magnetron sputtering (dcMS) and cathodic arc evaporation (CAE) in promoting substrate adhesion [4], film density [5], and surface smoothness [7], while avoiding the disadvantages from both of them like poor growth directionality, coarse columnar grain, and macroparticles. HiPIMS has already achieved great successes in microstructure modulation and property enhancement for thin films/coatings in laboratories [8]–[10]. However, its industrial application is still limited due to low deposition rate and discharge instability [11]–[13]. The loss of deposition rate attributes to the return of sputtered material ions back to target surface [14]. Meanwhile, discharge instability is also hard to avoid because HiPIMS works at abnormal glow region [16] which could easily transit into the arc region under high instant pulse voltage conditions [17]. Arcing on target surface will emit macrodroplets and degenerate thin films/coatings properties. These two features are the primary factors that need considering in HiPIMS applications.

According to specific applicable requirements, surface layers deposited by HiPIMS can be categorized into two main types: 1) surface protection coatings [18]–[20] and 2) functional thin films [7], [21], [22]. Surface protection coatings like transitional metal nitride/carbide are comprehensively deposited through dcMS or CAE methods. Their structures and properties are not quite sensitive to discharge instability unless pivotal mechanical damage caused by structural defects and property deterioration happens. Meanwhile, frequent arcing can be depressed by the advanced design of pulse unit [17]. However, the deposition rate of HiPIMS is much lower than dcMS, not even to mention CAE. Thus, although dense and refined grain nanocomposite coatings can be prepared by HiPIMS [8], [23], persuasion of coating customers turning into HiPIMS is not effective. However, low deposition rate does not matter so much to functional thin films, sometimes even becomes an advantage. Dutta *et al.* [25] reported that ultrathin Pt group metal films showed anomalous higher electric conductivity than Cu film. Film thickness can be controlled more precisely under low deposition rate conditions. Meanwhile, the high plasma density and ionization degree of sputtered atoms are beneficial to micronanoprocessing and the enhancement of film properties. For example, ions can be manipulated to fill or etch trenches and vias of semiconductor microprocessors [26], [27]. Ultrathin metal layers deposited by HiPIMS showed lower electrical resistivity than dcMS,

Manuscript received April 2, 2018; revised September 28, 2018; accepted December 20, 2018. This work was supported in part by the Project of the National Natural Science Foundation of China under Grant 11705258 and Grant 51522106, in part by the State Key Project of Fundamental Research of China under Grant 2017YFB0702303, in part by the Zhejiang Key Research and Development Program under Grant 2017C01001, in part by the Natural Science Foundation of Ningbo under Grant 2017A610012, and in part by the Cixi Municipal Key Technologies Research and Development Program under Grant 2015A07. The review of this paper was arranged by Senior Editor F. Taccogna. *(Corresponding authors: Peiling Ke; Aiying Wang.)*

X. Zuo, is with the Key Laboratory of Marine Materials and Related Technologies, Zhejiang Key Laboratory of Marine Materials and Protective Technologies, Ningbo Institute of Materials Technology and Engineering, Chinese Academy of Sciences, Ningbo 315201, China.

R. Chen is with the Key Laboratory of Marine Materials and Related Technologies, Zhejiang Key Laboratory of Marine Materials and Protective Technologies, Ningbo Institute of Materials Technology and Engineering, Chinese Academy of Sciences, Ningbo 315201, China, and also with the University of Chinese Academy of Sciences, Beijing 100049, China.

P. Ke and A. Wang are with the Key Laboratory of Marine Materials and Related Technologies, Zhejiang Key Laboratory of Marine Materials and Protective Technologies, Ningbo Institute of Materials Technology and Engineering, Chinese Academy of Sciences, Ningbo 315201, China, and also with the Center of Materials Science and Optoelectronics Engineering, University of Chinese Academy of Sciences, Beijing 100049, China (e-mail: kepl@nimte.ac.cn; aywang@nimte.ac.cn).

Color versions of one or more of the figures in this paper are available online at http://ieeexplore.ieee.org.

Digital Object Identifier 10.1109/TPS.2018.2889696

which has promising applications in microelectronics, space, and instrumentation technology [9], [28]. However, discharge instability like arcing would be vital for the properties of these kinds of thin films.

Therefore, considering the complex operation modes and particle transport processes [15], [29], [30], it is necessary to investigate the state-of-the-art operation ranges for various HiPIMS deposition applications. Helmersson and Samuelsson *et al.* [5] compared the deposition rate of eight different target materials (Al, Ti, Cr, Cu, Zr, Ag, Ta, and Pt) by HiPIMS with dcMS. Christie [14] analyzed the deposition rate for various sputtering targets by a pathway model. The ionization degree in the HiPIMS process with different targets under the same conditions differs. Moreover, Yushkov and Anders [6] found that gas breakdown in HiPIMS discharge was a function of the time to the previous discharge pulse. The discharge behaviors with various targets in HiPIMS need to be clarified. Herein, we will discuss the breakdown of Ar gas and discharge formation with Ag, Cu, Cr, Mo, Zr, Ti, and C targets. They are widely applied in the fabrication of diamond like carbon, carbon-based nanocomposites, and transitional metal nitride coatings. The sputter yield and ionization energy of these targets vary in large ranges. The voltage and current characteristics are analyzed to find the contribution of four processes on HiPIMS discharge, such as secondary electron emission, gas sputter, self-sputter, and ionization of sputtered materials. Especially the interactive influence of secondary electron emission yield, sputter yield and ionization energy on the ionization degree of sputtered materials are clarified. Optical emission spectroscopy (OES) further conforms the results of the analysis. Finally, a probable application scope of HiPIMS deposition concerning ionization degree of sputtered materials and deposition rate is suggested.

II. Experimental Setup and Target Current

A. Experimental Setup

Details about the HiPIMS equipment and target current measurement arrangements have been described in [16]. The dimensions of the cylindrical chamber are 60 cm in diameter and 60 cm in height. Background pressure for all experiments is pumped to 1.5×10^{-2} mTorr to avoid the influence from residual oxygen and water molecule to the utmost. Working pressure is set at 3.8 mTorr by 50-sccm research grade (99.999%) Ar gas. A pulse unit (HPPMS-20k, PTL) is used to power the magnetron. Pulsewidth and pulse frequency are 200 μs and 50 Hz, respectively. The targets (99.9% purity with the size of 40 cm × 10 cm × 0.7 cm) with various sputter yields are used to investigate target current behaviors with the variation of the pulse voltage. Gas sputter yield (Y_{Ar^+}) and self-sputter yield (Y_{self}) under different incident energy (E_i) ion bombardments are calculated by SRIM [31], which are plotted in Fig. 1. OES (Acton SpectraPro SP-2500, Princeton Instruments) is applied to characterize particle species and emission intensities, which scans from 200 to 900 nm with wavelength resolution of 1 nm. Although it is the plasma region near the substrate holder measured by OES, its results still could provide reliable references for discussion.

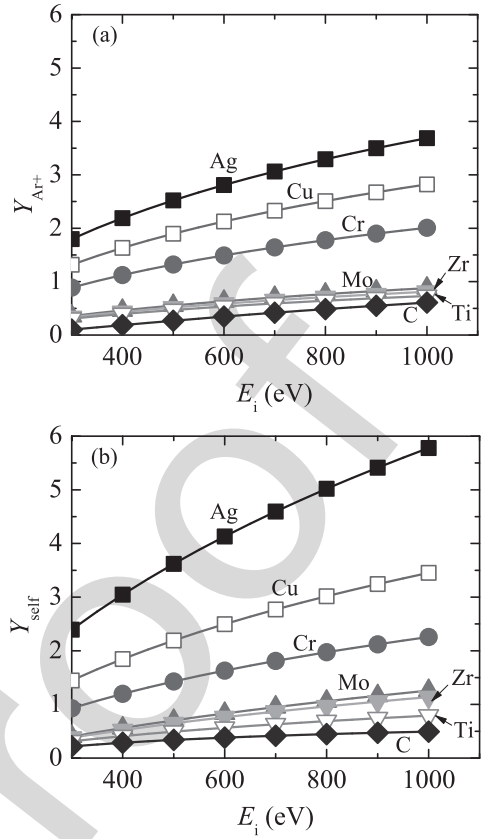

Fig. 1. (a) Sputter yield (Y_{Ar^+}) and (b) self-sputter yield (Y_{self}) of the targets under different incident ion energies (E_i). (Obtained by SRIM software.)

Meanwhile, it should be noted that the OES data just give qualitative information on HiPIMS discharge.

B. About Target Current

Average target currents (I_{ave}) during each pulse were calculated by the following formula:

$$I_{ave} = \frac{1}{T}\int_0^T I_t(t)dt \tag{1}$$

where T = 20 ms is the pulse period.

The target current generated from Ar^+ incidence (I_{Ar^+}), including ion current and secondary electron current, can be written in the following equation:

$$I_{Ar^+} = 0.5eSn_{Ar^+}(1+\gamma_{Ar^+})\sqrt{\frac{k_B T_e}{m_{Ar^+}}} \tag{2}$$

where e is the elementary charge, S is the area of racetrack, n_{Ar^+} is the density of Ar^+ ions, γ_{Ar^+} is the secondary electron emission yield under the bombardment of Ar^+, k_B is Boltzmann's constant, T_e is the electron temperature, and m_{Ar^+} is the mass of Ar^+. Current generated from sputtered material ions ($I_{M^{z+}}$) can also be written in similar equations as follows:

$$I_{M^{z+}} = \sum_{z=1,2} zeS\Gamma_{M^{z+}}(1+\gamma_{M^{z+}}) \tag{3}$$

$$\Gamma_{M^+} = 0.5\alpha(Y_{Ar^+}n_{Ar^+} + Y_{self}n_{M^+} + Y_{self}{}'n_{M^{2+}})\sqrt{\frac{k_B T_e}{m_{M^+}}} \quad (4)$$

$$\Gamma_{M^{2+}} = 0.5\beta(Y_{Ar^+}n_{Ar^+} + Y_{self}n_{M^+} + Y_{self}{}'n_{M^{2+}})\sqrt{\frac{k_B T_e}{m_{M^{2+}}}} \quad (5)$$

where $\Gamma_{M^{z+}}$ is the metal ion flux to the target, α ($0 < \alpha < 1$) is the first ionization degree of the target material, β is the second ionization degree, $Y_{self}{}'$ is self-sputter yield under M^{2+} ions, n_{M^+} and $n_{M^{2+}}$ are M^+ and M^{2+} density, respectively, and $m_{M^+} = m_{M^{2+}}$ is the target material ion mass. Therefore, the target current (I_t) can be obtained: $I_t = I_{Ar^+} + I_{M^{z+}}$. For simplicity, first, without considering the second ionization of sputtered material atoms, I_t can be written as the following form:

$$I_t = eS\Gamma_{Ar^+}\left(1 + \gamma_{Ar^+} + \frac{\alpha Y_{Ar^+}}{2 - \alpha Y_{self}}\sqrt{\frac{m_{Ar^+}}{m_{M^+}}}\right) \quad (6)$$

where Γ_{Ar^+} is the Ar^+ ion flux to target, which is expressed as follows:

$$\Gamma_{Ar^+} = 0.5n_{Ar^+}\sqrt{\frac{k_B T_e}{m_{M^+}}}. \quad (7)$$

III. Results and Discussion

A. Breakdown Voltage and Pulse Voltage Range of Different Targets in Ar HiPIMS

The current–voltage (*IV*) curves of HiPIMS with various targets are shown in Fig. 2. Pulse voltage is the set output voltage of the power supply, while voltage measured on the target by the oscilloscope is labeled as the target voltage. When the target voltage is high enough to ionize the Ar gas, gas breakdown and discharge occur. The breakdown voltages (U_b) of Ar gas in HiPIMS with different targets are distinct, which are plotted in Fig. 3. Breakdown voltage for graphite (C) target is the highest (721 V), while for Zr target is the lowest (356 V). The averaged target current increases with the improvement of the pulse voltage. However, too much high pulse voltage results in arc. The arcing voltages (U_{arc}) for each kind of targets are presented in Fig. 3. When the pulse voltage is higher than those values for a specific target, arcs generate. Thus, the stable work ranges of pulse voltage are obtained. Zr and Mo targets are sputtered in wider voltage ranges than others. Zr target can work in the largest voltage range, but the highest pulse voltage is achieved on the Mo target. In addition, Ti, Cu, and W targets can also work stably in large voltage ranges. However, Ag HiPIMS discharges easily transform from glow into arc.

As it is known, breakdown voltage is defined as the lowest voltage at which electric discharge occurs. It is determined by the work function (F) of the targets, which is the minimum energy needed to remove an electron from the target into the vacuum. Thus, it is expected that the variation of breakdown voltage with atomic number (Z) has a similar trend like work function. However, although the work function determines the breakdown voltage of various targets, it does not show a direct relationship with arcing voltage. In the process of glow discharge formation, energetic electrons emitted from target surface ionize Ar atoms in avalanche forms. In this stage, sputtering has not happened yet. When the generated ions are attracted back to bombard target surface energetically, sputtering happens. In HiPIMS discharge, the atoms emitted from the target surface are thought to be ionized overwhelmingly as compared to dcMS [1]. This process even can dominate in HiPIMS, which is able to cause severe self-sputter [30]. Discharge state in this stage is affected by target materials greatly. Therefore, arcing voltage would be influenced by the ionization of sputtered materials.

Meanwhile, no direct relationship between target current and sputter yield is observed as shown in Fig. 2. The averaged current is the lowest on Ag target that has the highest sputter yield. When the pulse voltage is 700 V, the average current of different targets is in the order from high to low as follows: Ti, Zr, Mo, Cu, Ag, and C. In addition, with the increase in pulse voltage, *IV* curves present different slopes which can be classified into two groups. For example, the Cu target current increases slowly after breakdown, and then, with the increase in pulse voltage, it becomes more and more fast until arc happens. However, the increase tendency of target current with pulse voltage for Ti is on the contrary. These differences from *IV* curves indicate that the secondary electron emission yield, gas sputter yield, self-sputter yield, and ionization energy will affect the discharge in HiPIMS interactively.

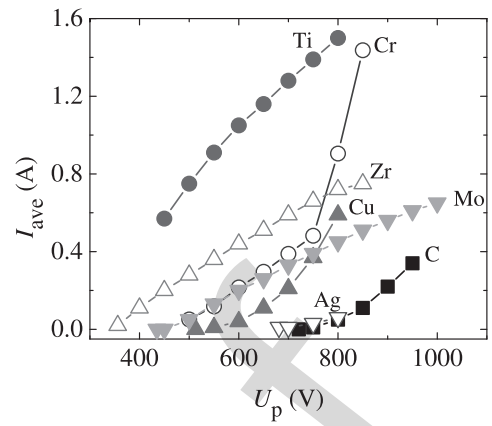

Fig. 2. Variations of averaged target current (I_{ave}) with pulse voltage (U_p) in HiPIMS discharges with different targets (measured).

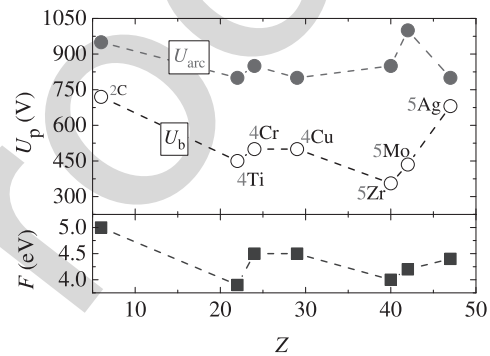

Fig. 3. Variation of breakdown voltage (U_b), arcing voltage (U_{arc}), and work function (F) with atomic number (Z).

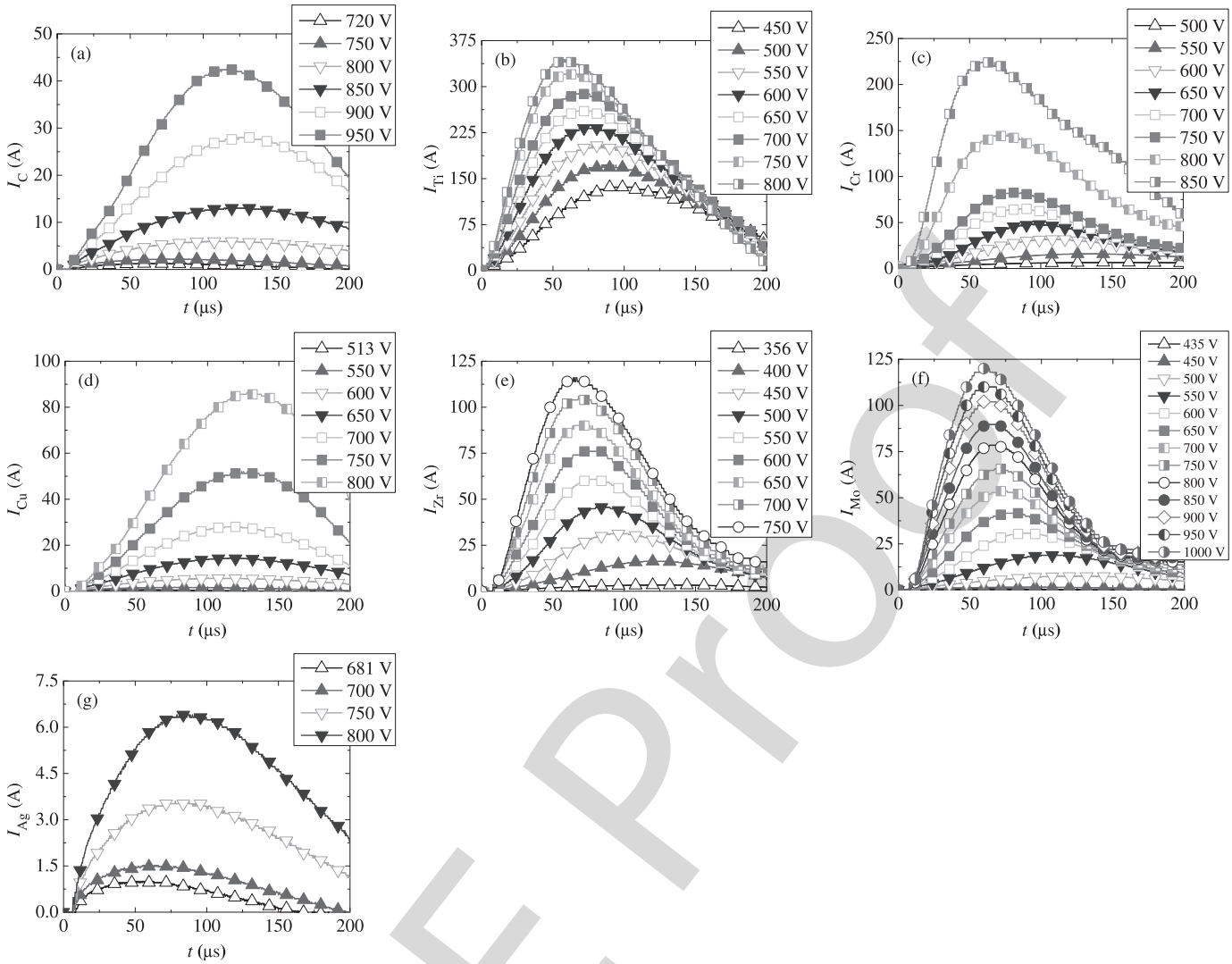

Fig. 4. Different target current waveforms in the pulse voltage ranges of stable HiPIMS discharges. Current measured on the C, Ti, Cr, Cu, Zr, Mo, and Ag targets is labeled as I_C, I_{Ti}, I_{Cr}, I_{Cu}, I_{Zr}, I_{Mo}, and I_{Ag}, respectively.

B. Variation of Current Waveform on Different Targets

The current waveforms on different targets during the 200-μs pulse-on time are demonstrated in Fig. 4. Apparently, all the target currents are transient. No stable current stage is observed. Although all the current waveforms present humplike shape, some details in current behaviors are distinct for different targets. First, I_{Zr} and I_{Mo} can nearly reach a stable low current stage at the end of relatively high-voltage pulse conditions ($\geq$500 and 600 V, respectively). Second, the time (Δt_{max}) of target current maximum (I_p) changes with pulse voltage and differs in target elements. Δt_{max} increases with the rise of pulse voltage on Cu and Ag targets but decreases on other targets in our experiments. Third, the target current at the same pulse voltage is also different. The current waveform is interactive resultant of ionization, gas sputter, self-sputter, and gas rarefaction processes. Its evolution under various conditions has been discussed in detail by many researchers [32]–[34]. Here, we focus on the target current maximum as it is a key parameter affecting the sputtering rate. Usually, high target current is preferred in HiPIMS unless arc generates. The highest current is obtained on Ti target in our experiments when the same pulse voltage (700 V) is applied. Details of target current waveform, including current maximum, Δt_{max}, increment rate (k_u), and decreasing rate (k_d) at 700 V for different targets, are presented in Fig. 5. The pulse voltage applied on the graphite target is selected as 720 V, because 700 V is insufficient for discharge formation. For targets with transitional metal in a subgroup (III or IV) or period (third or fourth), target current maximum decreases with the increase in atomic number. Fig. 5(b) shows the change of Δt_{max} with different atomic numbers. However, Fig. 5(b) does not show a similar trend like current maximum in Fig. 5(a). This could attribute to the ionization of sputtered materials. k_u and k_d are defined in the following equations:

$$k_u = \frac{I_p - 0}{\Delta t_{max}} \tag{8}$$

$$k_d = \frac{I_{end} - I_p}{200 - \Delta t_{max}} \tag{9}$$

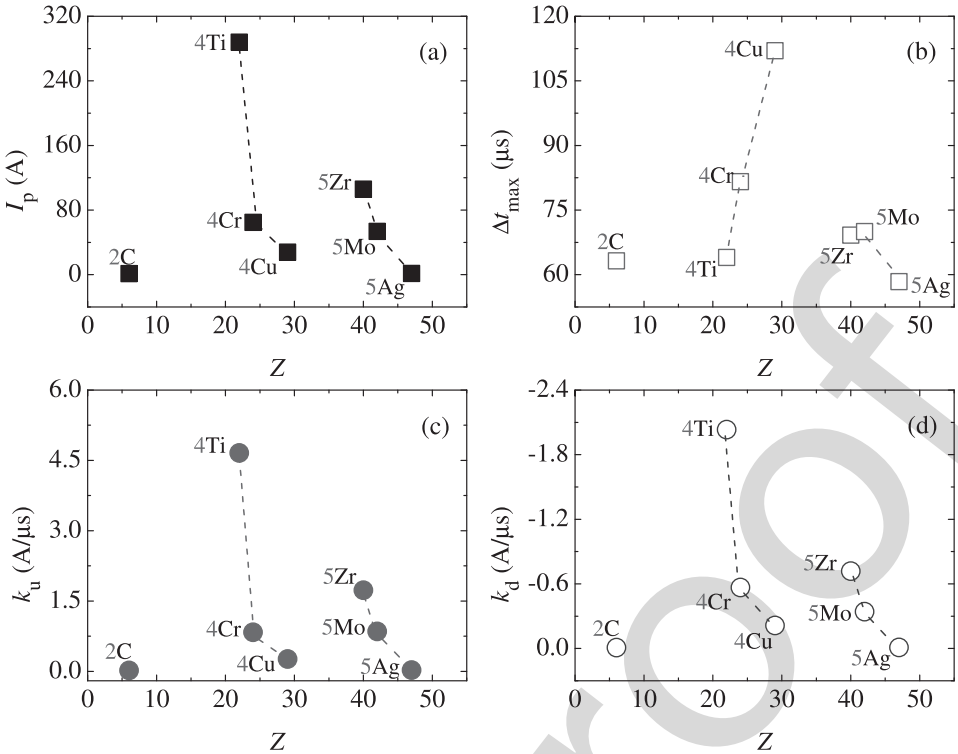

Fig. 5. Details on the current waveforms on different targets measured at with pulse voltage at 700 V, such as (a) current maximum (I_p), (b) corresponding time (Δt_{max}), (c) increase rate (k_u), and (d) decrease rate (k_d).

where I_{end} is the target current at the end of voltage pulse. As shown in (6), the rate of change in target current generally presents the ionization rate in HiPIMS discharge. It is found that for HiPIMS discharge with higher current maximum, the target current reaches maximum faster, but also decreases earlier. k_u and k_d also obey periodic feature like I_p. Generally, k_d is smaller than k_u. The change trend of them with atomic number is similar with the secondary electron emission yield except Ti.

When working pressure and pulse voltage are the same, secondary electron emission yield on different targets will lead to significant distinct in plasma density in HiPIMS. Thus, the dose of incident Ar^+ on the targets changes with different target elements. The incident Ar^+ generates new electrons and sputters target atoms out. The sputtered atoms will also be ionized in HiPIMS plasma. The target current is a sum of conductive electron current and ion current. Ion current composes of Ar^+ current and target material ions current. There would be monovalent and bivalent ions of target material according to first ionization energy ($E_{0\to1}$) and second ionization energy ($E_{1\to2}$). The electron current on the target surface is generated from Ar^+ and target material ions. The density of target material ions is influenced by Y_{Ar^+}, Y_{self}, $E_{0\to1}$, and $E_{1\to2}$. When we analyze the target current, the difference in secondary electron emission yield is considered first. Fig. 6 figures out the change of secondary electron emission yield (γ_{SEEY}) with atomic number corresponding to different target materials. The incident ion energy is assumed to be 700 eV when the pulse voltage is 700 V. As the energy per atomic mass number is less than 300 eV, secondary electron emission is determined by the potential energy (E_p) of incident ions [30]. Therefore, the secondary electron yield from ion bombardment can be calculated by the following equation:

$$\gamma_{SEEY} = 0.032 * (0.78E_p - 2F). \tag{10}$$

The values of work function (F) and potential energy (E_p) for different materials are listed in Table I. As shown in Fig. 6(a), with the increase in atomic number in a subgroup or period, γ_{Ar^+} has a similar trend like the target current maximum in Fig. 5(a). It means that the electron current generated by Ar^+ incidence is dominant. However, when carefully comparing γ_{Ar^+} of the elements from the fourth period with that of the fifth period, Zr HiPIMS should have the highest target current at the same pulse voltage. However, current on Ti target is the highest; meanwhile, Cr and Cu

TABLE I

F, FIRST, AND SECOND IONIZATION ENERGIES FOR VARIOUS MATERIALS

Element	F (eV)	$E_{0\to1}$ (eV)	$E_{1\to2}$ (eV)
Ar	N/A	15.76	27.63
C	4.5	11.26	24.38
Ti	3.9	6.83	13.58
Cr	4.5	6.77	16.5
Cu	4.9	7.73	20.29
Zr	4.0	6.63	13.16
Mo	4.2	7.09	16.17
Ag	4.4	7.58	21.45

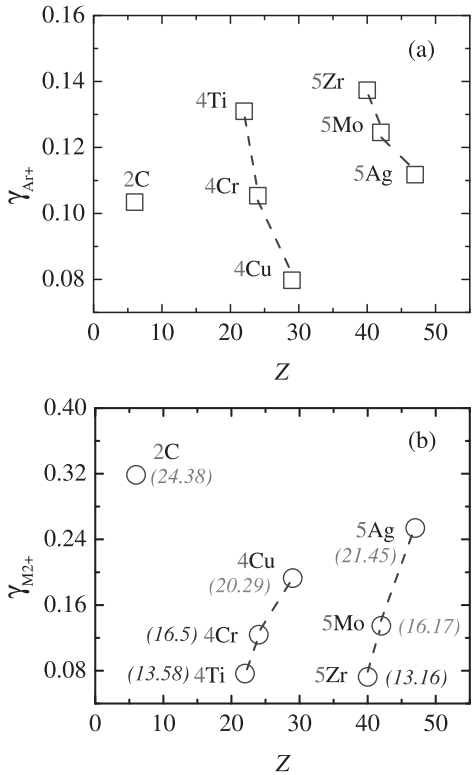

Fig. 6. Secondary electron emission yield (γ_{SEEY}) of various targets under the bombardment of (a) Ar^+ ions and (b) bivalent target material ions (M^{2+}).

HiPIMS also have higher target current than Mo and Ag HiPIMS, respectively. Since the monovalent ions are unable to cause secondary electron emission, the existence of bivalent target material ions is further considered. The first ionization energy of Ar is 15.76 eV, and target material atoms with the second ionization energy lower than 15.76 eV, like Ti and Zr, can be ionized into bivalent ions with high probability. In addition, there are Cr and Mo that have the second ionization energies near around 15.76 eV. These sputtered materials participated in discharge processes and are partially ionized. Therefore, different sputter yield and ionization degrees would also contribute to the variation deviation of target current maximum from γ_{Ar^+}.

C. Relationship Between Ionization Degree and Peak Target Current

As the working pressure is set at 3.8 mTorr, the mean free path is larger than cathode sheath thickness. Therefore, when the pulse voltage is 700 V, it is reasonable to assume that the energy of incident ions is 700 eV as the second ionization process is neglected. Gas sputter yield and self-sputter yield of various targets with incident energy at 700 eV can be found in Fig. 1. Self-sputter yield is higher than the gas sputter yield. The difference between them is distinct according to the kind of target material. For Ag and Cu targets, the self-sputter yield is much higher than gas sputter yield when compared with others. It could be speculated that the target material with high ionization degree, self-sputter yield, and low ionization energy

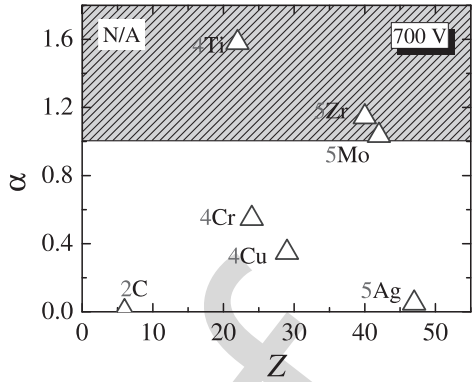

Fig. 7. Calculated ionization degree (α) of various target materials. The second ionization process exists when α is larger than 1.

prefers the state-of-the-art HiPIMS with high deposition rate and stability.

As the target current is transit, the ionization degree of sputtered materials is also expected to vary with time. The ionization degree can be calculated through the ionization region model [33]. The cross section data of excitation, ionization, deexcitation, and combination processes for different species can be found in reaction databases, such as from the OpenADAS database [35]. When the pulse voltage and working pressure are 700 V and 3.8 mTorr, the maximums of ionization degree (α) calculated from different target currents are presented in Fig. 7. According to these maximums of ionization degree, target materials can be categorized into three kinds: 1) Ag and C targets, the maximum ionization degree is less than 10%; 2) 55% and 35% for Cr and Cu; and 3) higher than 100% for Ti, Zr, and Mo. The ionization energy of C atom is the highest, thus its ionization degree is the lowest. However, the ionization energy of Ag atom is lower than that of Cu atoms, but its ionization degree is also very low. This phenomenon can be attributed to its high sputter yield, a large amount of Ag atoms participate in discharge which would reduce the electron temperature. Therefore, the target with high sputter yield will have a reduced ionization degree. Ionization degree higher than 100% is impossible, and these results are attributed to that only the first ionization processes are considered and bivalent ions are neglected. It is easy to deduce that the second ionization process exists in Ti, Zr, and Mo HiPIMS. Therefore, it is expectable to control the incident particles' energy to design dense, fine grain, and nanocomposite films for Cr, Ti, Zr, and Mo targets but obtain relatively high deposition rate for Ag and Cu targets in HiPIMS deposition process. For the high ionization energy and low sputter yield target C, other methods should be introduced to improve ionization degree [36] or deposition rate [37]. These results can also be explored to other targets according to their secondary electron emission yield, sputter yield, and ionization degree with the exception of ferromagnetic materials such as Fe, Co, and Ni.

D. Optical Emission Spectra of C, Cr, and Ti HiPIMS Plasma

According to the first and second ionization of sputtered atoms, OES spectra for HiPIMS with three different targets

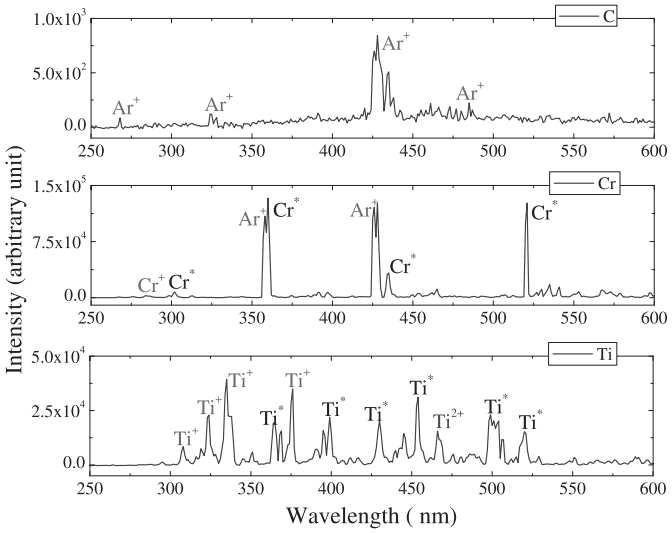

Fig. 8. OES spectra of C, Cr, and Ti HiPIMS discharge.

are detected, such as high first ionization energy element C, low second ionization energy element Ti, and high sputter yield element Cr. Correspondingly, the pulse voltage and pressure for OES measurements are 700 V and 3.8 mTorr, respectively. All the parameters of the spectroscope are set the same so that the measured OES spectra can be comparable with each other. The results are plotted in Fig. 8. C atom spectrum cannot be found. A weak spectrum peak of CrII 284 nm appears in the OES spectra of Cr HiPIMS discharge. As predicted from the ionization degree analysis, TiIII 466 nm of bivalent Ti^{2+} ions were observed in Ti HiPIMS.

IV. Conclusion

The discharge behaviors of HiPIMS have been investigated on Ag, Cu, Cr, Mo, Zr, Ti, and C targets. The breakdown voltage is determined by the work function of the target element, but the arcing voltage is also affected by the ionization of sputtered atoms. Stable discharge ranges of these targets are found. High Γ_{SEEY} results in low breakdown voltage and high discharge current, and vice versa. HiPIMS discharge with Ti, Mo, and Zr targets is not easy to arc at high voltage. An analytical current model was used to analyze the interactive influence of the secondary electron emission yield, sputter yield, and ionization energy on the ionization degree of sputtered atoms. The results show that the target materials with relatively low ionization energy and sputter yield, such as Cr, Ti, Zr, and Mo, tend to have higher ionization degree. Targets with high sputter yield like Ag and Cu have low ionization degree. The second ionization of sputtered atoms happens in Ti, Zr, and Mo HiPIMS. However, high sputter yield elements like Ag and Cu have relatively low ionization degree.

References

[1] D. Lundin, M. Čada, and Z. Hubička, "Ionization of sputtered Ti, Al, and C coupled with plasma characterization in HiPIMS," *Plasma Sources Sci. Technol.*, vol. 24, p. 035018, Jun. 2015.

[2] A. Hecimovic and A. P. Ehiasarian, "Time evolution of ion energies in HIPIMS of chromium plasma discharge," *J. Phys. D: Appl. Phys.*, vol. 42, no. 13, p. 135209, 2009.

[3] U. Helmersson, M. Lattemann, J. Bohlmark, A. P. Ehiasarian, and J. T. Gudmundsson, "Ionized physical vapor deposition (IPVD): A review of technology and applications," *Thin Solid Films*, vol. 513, pp. 1–24, Aug. 2006.

[4] Z. Wang, D. Zhang, P. Ke, X. Liu, and A. Wang, "Influence of substrate negative bias on structure and properties of TiN coatings prepared by hybrid HIPIMS method," *J. Mater. Sci. Technol.*, vol. 31, no. 1, pp. 37–42, 2015.

[5] M. Samuelsson, D. Lundin, J. Jensen, M. A. Raadu, J. T. Gudmundsson, and U. Helmersson, "On the film density using high power impulse magnetron sputtering," *Surf. Coat. Technol.*, vol. 205, no. 2, pp. 591–596, 2010.

[6] G. Y. Yushkov and A. Anders, "Origin of the delayed current onset in high-power impulse magnetron sputtering," *IEEE Trans. Plasma Sci.*, vol. 38, no. 11, pp. 3028–3034, Nov. 2010.

[7] F. Cemin *et al.*, "Epitaxial growth of Cu(001) thin films onto Si(001) using a single-step HiPIMS process," *Sci. Rep.*, vol. 7, May 2017, Art. no. 1655.

[8] P. Souček *et al.*, "Superhard nanocomposite nc-TiC/aC:H coatings: The effect of HiPIMS on coating microstructure and mechanical properties," *Surf. Coat. Technol.*, vol. 311, pp. 257–267, Feb. 2017.

[9] F. Cemin, D. Lundin, D. Cammilleri, T. Maroutian, P. Lecoeur, and T. Minea, "Low electrical resistivity in thin and ultrathin copper layers grown by high power impulse magnetron sputtering," *J. Vac. Sci. Technol. A, Vac., Surf., Films*, vol. 34, no. 5, p. 051506, 2016.

[10] X. Qin, P. Ke, A. Wang, and K. H. Kim, "Microstructure, mechanical and tribological behaviors of MoS_2-Ti composite coatings deposited by a hybrid HIPIMS method," *Surf. Coat. Technol.*, vol. 228, pp. 275–281, Aug. 2013.

[11] P. Raman, J. Weberski, M. Cheng, I. Shchelkanov, and D. N. Ruzic, "A high power impulse magnetron sputtering model to explain high deposition rate magnetic field configurations," *J. Appl. Phys.*, vol. 120, no. 16, p. 163301, 2016.

[12] N. Brenning *et al.*, "Understanding deposition rate loss in high power impulse magnetron sputtering: I. Ionization-driven electric fields," *Plasma Sources Sci. Technol.*, vol. 21, no. 2, p. 025005, 2012.

[13] K. Yukimura, R. Mieda, H. Tamagaki, and T. Okimoto, "Electrical characteristics of arc-free high-power pulsed sputtering glow plasma," *Surf. Coat. Technol.*, vol. 202, pp. 5246–5250, Aug. 2008.

[14] D. J. Christie, "Target material pathways model for high power pulsed magnetron sputtering," *J. Vac. Sci. Technol. A, Vac., Surf., Flims*, vol. 23, no. 2, pp. 330–335, 2005.

[15] N. Brenning, J. T. Gudmundsson, M. A. Raadu, T. J. Petty, T. Minea, and D. Lundin, "A unified treatment of self-sputtering, process gas recycling, and runaway for high power impulse sputtering magnetrons," *Plasma Sources Sci. Technol.*, vol. 26, no. 12, p. 125003, 2017.

[16] X. Zuo, P. Ke, R. Chen, X. Li, M. Odén, and A. Wang, "Discharge state transition and cathode fall thickness evolution during chromium HiPIMS discharge," *Phys. Plasmas*, vol. 24, p. 083507, Jul. 2017.

[17] D. J. Christie, F. Tomasel, W. D. Sproul, and D. C. Carter, "Power supply with arc handling for high peak power magnetron sputtering," *J. Vac. Sci. Technol. A, Vac., Surf., Films*, vol. 22, no. 4, pp. 1415–1419, 2004.

[18] X. Tian, Y. Ma, J. Hu, M. Bi, C. Gong, and P. K. Chu, "Microstructure and mechanical properties of $(AlTi)_xN_{1-x}$ films by magnetic-field-enhanced high power impulse magnetron sputtering," *J. Vac. Sci. Technol. A, Vac., Surf., Films*, vol. 35, p. 021402, Mar. 2017.

[19] S. Danaher, T. Dudziak, P. K. Datta, R. Hasan, and P. S. Leung, "Long-term oxidation of newly developed HIPIMS and PVD coatings with neural network prediction modelling," *Corrosion Sci.*, vol. 69, pp. 322–337, Apr. 2013.

[20] K. D. Bakoglidis *et al.*, "Comparative study of macro- and microtribological properties of carbon nitride thin films deposited by HiPIMS," *Wear*, vols. 370–371, pp. 1–8, Jan. 2017.

[21] A. Aijaz, Y.-X. Ji, J. Montero, G. A. Niklasson, C. G. Granqvist, and T. Kubart, "Low-temperature synthesis of thermochromic vanadium dioxide thin films by reactive high power impulse magnetron sputtering," *Sol. Energy Mater. Sol. Cells*, vol. 149, pp. 137–144, May 2016.

[22] M. Mickan, U. Helmersson, H. Rinnert, J. Ghanbaja, D. Müller, and D. Horwat, "Room temperature deposition of homogeneous, highly transparent and conductive Al-doped ZnO films by reactive high power impulse magnetron sputtering," *Sol. Energy Mater. Sol. Cells*, vol. 157, pp. 742–749, Dec. 2016.

[23] Q. Ma, L. Li, Y. Xu, J. Gu, L. Wang, and Y. Xu, "Effect of bias voltage on TiAlSiN nanocomposite coatings deposited by HiPIMS," *Appl. Surf. Sci.*, vol. 392, pp. 826–833, Jan. 2017.

[24] D. Lundin, J. Jensen, and H. Pedersen, "Influence of pulse power amplitude on plasma properties and film deposition in high power pulsed plasma enhanced chemical vapor deposition," *J. Vac. Sci. Technol. A, Vac., Surf., Films*, vol. 32, p. 030602, Mar. 2014.

[25] S. Dutta *et al.*, "Thickness dependence of the resistivity of platinum-group metal thin films," *J. Appl. Phys.*, vol. 122, p. 025107, Jul. 2017.

[26] A. Anders, "Metal plasmas for the fabrication of nanostructures," *J. Phys. D: Appl. Phys.*, vol. 40, no. 8, p. 2272, 2007.

[27] H. L. Brown, S. A. Thornley, S. J. Wakeham, M. J. Thwaites, R. J. Curry, and M. A. Baker, "The impact of substrate bias on a remote plasma sputter coating process for conformal coverage of trenches and 3D structures," *J. Phys. D: Appl. Phys.*, vol. 48, no. 33, p. 335303, 2015.

[28] A. A. Solovyev, V. A. Semenov, V. O. Oskirko, K. V. Oskomov, A. N. Zakharov, and S. V. Rabotkin, "Properties of ultra-thin Cu films grown by high power pulsed magnetron sputtering," *Thin Solid Films*, vol. 631, pp. 72–79, Jun. 2017.

[29] K. Sarakinos, J. Alami, and S. Konstantinidis, "High power pulsed magnetron sputtering: A review on scientific and engineering state of the art," *Surf. Coat. Technol.*, vol. 204, no. 11, pp. 1661–1684, 2010.

[30] A. Anders, J. Andersson, and A. Ehiasarian, "High power impulse magnetron sputtering: Current-voltage-time characteristics indicate the onset of sustained self-sputtering," *J. Appl. Phys.*, vol. 102, no. 11, p. 113303, 2007.

[31] J. F. Ziegler, M. D. Ziegler, and J. P. Biersack, "SRIM—The stopping and range of ions in matter (2010)," *Nucl. Instrum. Methods Phys. Res. B, Beam Interact. Mater. At.*, vol. 268, pp. 1818–1823, Jun. 2010.

[32] Z. Wu *et al.*, "Discharge current modes of high power impulse magnetron sputtering," *AIP Adv.*, vol. 5, no. 9, p. 097178, 2015.

[33] M. Raadu, I. Axnäs, J. T. Gudmundsson, C. Huo, and N. Brenning, "An ionization region model for high-power impulse magnetron sputtering discharges," *Plasma Sources Sci. Technol.*, vol. 20, no. 6, p. 065007, 2011.

[34] B. C. Zheng, Z. L. Wu, B. Wu, Y. G. Li, and M. K. Lei, "A global plasma model for reactive deposition of compound films by modulated pulsed power magnetron sputtering discharges," *J. Appl. Phys.*, vol. 121, no. 17, p. 171901, 2017.

[35] H. P. Summers and M. G. O'Mullane, "Atomic data and modelling for fusion: The ADAS project," in *Proc. AIP Conf.*, vol. 1, 2011, pp. 179–187.

[36] A. Aijaz *et al.*, "Synthesis of hydrogenated diamondlike carbon thin films using neon–acetylene based high power impulse magnetron sputtering discharges," *J. Vac. Sci. Technol. A, Vac., Surf., Films*, vol. 34, no. 6, p. 061504, 2016.

[37] M. Hiratsuka, A. Azuma, H. Nakamori, Y. Kogo, and K. Yukimura, "Extraordinary deposition rate of diamond-like carbon film using HIPIMS technology," *Surf. Coat. Technol.*, vol. 229, pp. 46–49, Aug. 2013.

Xiao Zuo received the B.S. degree in physics from Hunan Normal University, Changsha, China, in 2009, and the Ph.D. degree in plasma physics from the Institute of Plasma Physics, Chinese Academy of Sciences, Hefei, China, in 2014.

His current research interests include high-power impulse magnetron sputtering discharge, plasma diagnosis, and simulation.

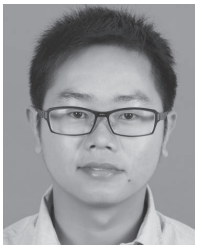

Rende Chen received the B.S. degree in communication engineering from the Beijing Institute of Petrochemical Technology, Beijing, China, in 2010, and the M.S. degree in material science and engineering from the University of Chinese Academy of Sciences, Beijing, China.

He is currently with the Ningbo Institute of Material Technology and Engineering, Chinese Academy of Sciences, Ningbo, China, where he is involved in the research work. His current research interests include vacuum technologies and plasma diagnosis.

Peiling Ke received the Ph.D. degree from the Institute of Metal Research, Chinese Academy of Sciences, Shenyang, China, in 2006.

Her current research interests include novel solid lubricant materials, MAX phase coatings, high-power impulse magnetron sputtering coating processes, and so on.

Aiying Wang received the B.S. degree in material science and engineering from Northwestern Polytechnical University, Xi'an, China, in 1998, and the Ph.D. degree from the Institute of Metal Research, Chinese Academy of Sciences, Shenyang, China, in 2003.

Her current research interests include advanced carbon-based materials, materials simulation, plasma surface engineering, and so on.